NURETH14-627

A COMPUTATIONAL STUDY ON INSTRUMENTATION GUIDE TUBE FAILURE DURING A SEVERE ACCIDENT IN BOILING WATER REACTORS

Walter Villanueva, Chi-Thanh Tran*, and Pavel Kudinov
Division of Nuclear Power Safety, Royal Institute of Technology (KTH), Stockholm, Sweden
*Present address: Institute of Energy, 6 Ton That Tung, Dong Da, Hanoi, Vietnam

Abstract

This paper focuses on the nature and timing of Instrumentation Guide Tube (IGT) failure in case of severe core melt accident in a Nordic type Boiling Water Reactor (BWR). First, a 2D structural analysis of a RPV lower head is performed to determine global vessel deformation, timing and mode of failure. Next, a structural analysis is also performed on a 3D IGT section taking into account the influence of global vessel deformation and thermo-mechanical load from the melt pool. We have found that the IG tube was not clamped in the housing at the time when welding ring of the IGT nozzle has been melted and global failure of the vessel wall has not started yet. This suggests that IGT failure is the dominant failure mode in the considered case of a large (~200 tons) melt pool.

Introduction

Ex-vessel accident termination and melt coolability in a deep water pool located under the reactor vessel are adopted in severe accident management strategy in Nordic Boiling Water Reactors (BWR). It is assumed that core melt ejected from the reactor pressure vessel will fragment, quench and form a coolable by natural circulation porous debris bed. Apparently, melt fragmentation and resulting characteristics of the debris bed [1, 2, 3, 4] and coolability [5] are contingent upon the mode of the vessel failure (rupture size and location, characteristic time of melt ejection from the vessel, melt composition, amount and superheat, etc.). Non-coolable debris will be dried out, reheated, re-melted and will attack containment base-mat, presenting a threat to containment integrity. Energetic molten fuel-coolant interaction (steam explosion) in a deep reactor cavity is also sensitive to melt discharge conditions [6] and creates another source of credible threat to containment integrity. The success of ex-vessel accident termination is majorly dependent on the melt ejection characteristic, which are currently too uncertain to establish on a firm basis that containment integrity can be preserved. Therefore reduction of uncertainties in the in-vessel stage of the accident is the aim of the present work.

Cooling of the CRGTs by means of standard crude purge flow is considered as one of the potentially effective severe accident mitigation measures that influences the in-vessel accident progression and affects vessel failure mode. CRGTs can survive melt attack when cooled from the inside and also help to remove some part of the decay heat generated in the melt pool.

A 2D coupled thermo-mechanical creep analysis has been performed previously [7] for the FOREVER experiment (a scaled model of a PWR) in order to investigate global failure mode

and predict failure time. A similar study [8] has focused on analysis of the global failure of a BWR vessel wall under thermo-mechanical load inflicted by a melt pool. It was found that the amount of melt has an effect on the global vessel failure mode, i.e., ballooning or localized creep. Another group of vessel failure modes is failure of the local penetrations such as nozzles of Instrumentation Guide Tube (IGT), Control Rod Guide Tube (CRGT), and pump. Previous work by Rempe et al. [9] addressed different failure mechanisms of the lower head that include IGT failure by either rupture or ejection. At system pressure below 2 MPa (typical in depressurized BWRs), IGT failure was found as the dominant failure mode, however there is an uncertainty if IGT fails by rupture or ejection. Another study [10] also addressed different failure mechanisms in the lower head by a thermo-mechanical analysis and supported the hypothesis that the welds of the penetration nozzle will fail first. However, no CRGT cooling was taken into account and no analysis of potential IGT clamping in the housing was performed. Therefore, a detailed analysis is needed to investigate possible clamping of the IGT as a means to prevent early IGT ejection. Our previous work with a shallower pool along with the study in this paper for a larger pool showed that the amount of melt in the lower head can have a significant effect on whether the IGT is clamped or not.

The goal of this work is to clarify if the IGT might fail before the occurrence of a global vessel wall failure. This is contingent upon (i) timing of the IGT nozzle welding failure, (ii) timing of possible IGT clamping in the narrow gap of the IGT housing flow limiter, and (iii) timing of the global vessel failure.

Coupled thermo-mechanical creep analyses of the RPV lower head and an IGT section are performed for a Nordic BWR design of the lower plenum. Deformation of the vessel wall are assumed to have negligible effect on the melt pool heat transfer, therefore only one way coupling is employed. Debris bed heat-up, re-melting, melt pool formation, and heat transfer are predicted with the Phase-change Effective Convectivity Model (PECM) [11]. The PECM is implemented on the platform of Fluent code [12]. Transient heat transfer characteristics predicted by PECM are provided for thermo-mechanical strength calculations. The creep analysis is performed using commercial code ANSYS [13], taking into account both the thermal and integral mechanical loads on the RPV. Material properties of the ABB-Atom reactor vessel [9] are used as an input data for the creep analysis.

A series of calculations were performed coupling a deep melt-pool behavior to vessel steel wall thermo-mechanical creep analyses. Thermal and mechanical load from the melt pool are used as boundary conditions for two consecutive thermo-mechanical creep analyses. First, a 2D structural analysis of a pressure vessel lower head is performed to determine the global vessel deformation, timing and mode of failure. We have found a localized creep mode of global vessel wall failure where creep strains are concentrated in the vicinity of the uppermost region of the melt pool. Next, a structural analysis is also performed on a 3D IGT section taking into account the influence of global vessel deformation and thermo-mechanical load from the pool. Given a certain melt pool depth and location of the IGT section, we have found that the IGT section did not clamp in the IGT housing flow limiter until global failure of the vessel wall and failure of the IGT nozzle welding, which implies that IGT failure is the dominant failure mode for a deep melt pool.

The paper structure is as follows. Section 2 discusses the thermal and mechanical aspects of the analysis including the creep modeling. In Section 3, results of succeeding calculations of global vessel wall deformation and failure and IGT failure are presented. Concluding remarks are provided in Section 4.

1. Computational treatment

In this section we provide details of the codes and models used to resolve different key physics at different scales in order to achieve a solution of a safety analysis problem. We divide this section into two parts: the thermal and mechanical aspects of the analysis and next the inclusion of creep. Two successive coupling procedures between PECM and ANSYS are performed. First, thermo-mechanical creep analysis of the reactor pressure vessel lower head is implemented in ANSYS. The PECM is used to calculate the transient thermal load from the melt pool to the vessel wall that is applied as a thermal boundary condition in the structural analysis. Second, global vessel deformations from the structural analysis (performed with ANSYS) of the vessel lower-head and local temperature field on the inner surface of the vessel (predicted by PECM) are used to investigate local thermo-mechanical behavior of an IGT section and define timing of possible clamping of the IGT in its housing.

1.1 Thermal and mechanical aspects

1.1.1 Material properties

The material properties of the vessel steel SA533B1 such as density, elastic modulus (linear isotropic), thermal conductivity (isotropic), specific heat, and coefficient of thermal expansion, which are all functions of temperature taken from Rempe et al. [9]. The Poisson's ratio is set to 0.3. It is important to note that the elastic modulus is very sensitive to temperature and that it decreases 2 orders of magnitude as the temperature increases from 300 to 1050 K. Consequently, as the elastic response of the material is inversely proportional to the elastic modulus, the strain due to creep increases significantly at high temperatures.

1.1.2 Model geometries and meshes

Two succeeding thermo-mechanical creep analyses have been performed. First, a 2D model of a typical Nordic BWR design lower plenum is considered to determine global vessel wall deformation and failure (see Figure 1). Next, a 3D IGT section is analyzed (see Figure 3) to determine the nature and timing of its failure.

The element type used for the global vessel wall structural analysis in ANSYS 13 [14] is Quad Plane223 which is a 2D 8-node coupled-field (structural-thermal) solid. For full transient analyses, a strong structural-thermal coupling is supported. The 2D geometry is meshed with 850 quadrilateral elements and 2901 nodes with an average edge length of 40 mm. A typical run of few thousands seconds of physical time with this mesh and a time-step of 10 s on an Intel Core 3GHz Linux platform takes about 0.8 h.

For the 3D IGT section structural analysis, the element type used in ANSYS 13 is Solid 226 which is a 3D 20-node coupled-field (structural-thermal) solid. Full transient analysis with a strong structural-thermal coupling is also implemented. The 3D geometry is meshed with 11553 tetrahedral elements and 18435 nodes with an average edge length of 15 mm. A typical run with this mesh and a time-step of 10 s on a similar platform as in the previous calculation takes about 10 h.

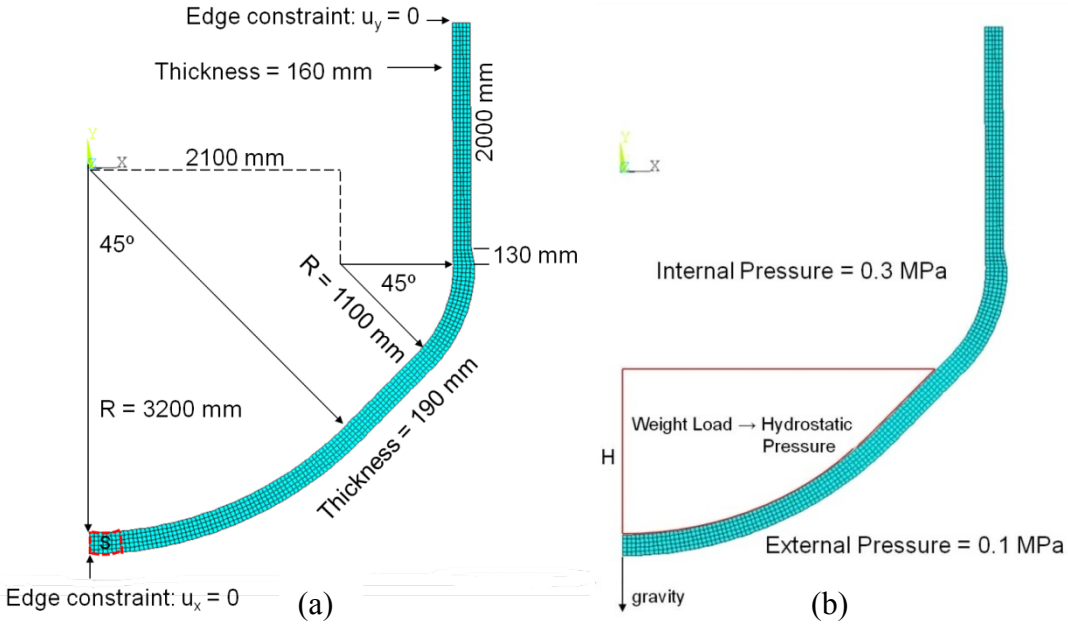

Figure 1. (a) 2D axisymmetric geometry and mesh with 850 quadrilateral elements and 2901 nodes, and (b) mechanical load on the reactor vessel.

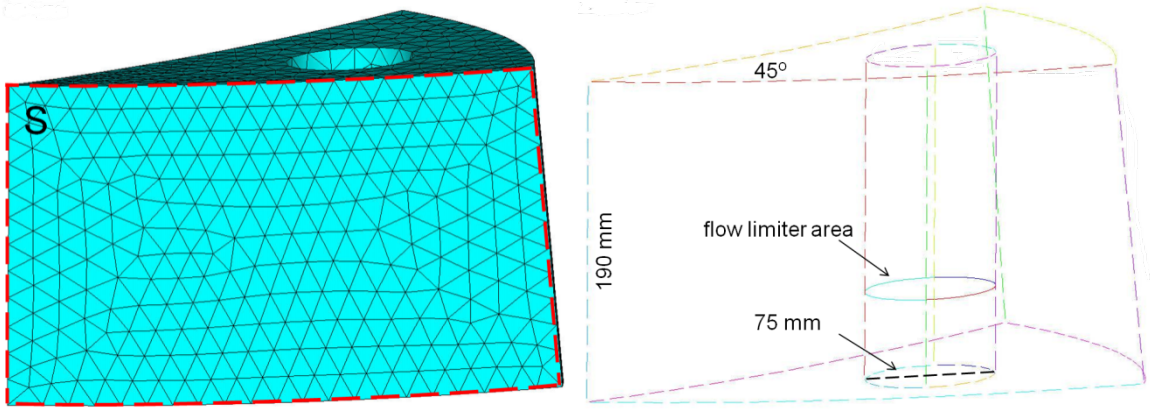

Figure 3. (a) Mesh of the 3D instrumentation guide tube section with 11553 tetrahedral elements and 18435 nodes, and (b) geometry with the location of the flow limiter.

Elmir L
Delete

1.1.3 Boundary conditions and other input parameters

Mechanical strength of the vessel wall depends on the thermal loads imposed on its boundaries. In the present work the PECM, i.e. the phase-change Effective Convectivity Model (ECM) is used for prediction of transient thermal loads imposed on the vessel wall from a decay-heated debris bed and melt pool formed in the BWR lower head during a severe accident. The ECM employs the concept of effective convectivity that was implemented first in the Effective Convectivity Conductivity Model (ECCM) developed by Bui and Dinh [15]. The ECM is a model for description of turbulent natural convection heat transfer in an internally heated fluid volume [11]. In the ECM method, the convective terms of the energy conservation equation are described using characteristic velocities; therefore the need of solving Navier-Stokes equations is eliminated. The characteristic velocities are determined using experimental heat transfer correlations, namely the upward, sideward and downward Steinberner-Reineke correlations [16]. The ECM is implemented in the commercial code

Fluent, to utilize advantages of pre- and post-processing of the data.

To describe phase-change heat transfer, the ECM was extended to Phase-change ECM (PECM). The main idea of the PECM is to use the reduced characteristic velocities to describe heat transfer in a mushy zone of non-eutectic melt mixture. Due to its computational efficiency, the PECM enables simulations of long transients of melt pool formation heat transfer during the accident progression in a realistic geometry of the lower-head with cooled CRGTs.

The ECM and PECM have been validated against a set of experiments which cover a broad spectrum of physical phenomena involved in melt pool formation heat transfer, and wide range of Rayleigh number. The ECM and PECM have been demonstrated as sufficiently accurate and computationally efficient tools for 3D simulations of melt pool formation heat transfer for a BWR accident analysis [17].

In the present work PECM simulations are performed for a 3D slice of BWR lower plenum. The slice geometry is a segment of BWR lower plenum, filled with decay-heated corium, including 6 cooled CRGTs connected from below with the vessel wall. It is assumed that a debris bed is formed in the lower plenum, the debris bed is heated up and re-melted due to inadequate cooling. The CRGTs are cooled from inside by water flow. The water is assumed to be ejected from the top outlet of CRGTs providing a water layer above the top surface of the debris bed. The boundary conditions applied for the simulation cases are as follows. The top and CRGTs walls are applied to Dirichlet boundary conditions, i.e. isothermal with water saturation temperature. Other surfaces are applied to Neumann boundary conditions. The external surface of the vessel wall is insulated therefore a small heat flux (20 W/m^2) is applied. Resulting transient thermal loads on the vessel wall are then used for the thermo-mechanical creep analysis. The effect of thermo-mechanical creep of the reactor vessel such as vessel displacements on the melt pool thermal analysis is not considered here.

1.2 Creep model and validation

In this section, we provide description of the creep model and parameters used in the calculation as well as the curve fitting of the experimental creep data. It is well known that stress and temperature can affect significantly the creep rate of structural materials. A typical creep curve consists of three stages before rupture, namely, the primary stage (also called transient creep), secondary (steady creep), and tertiary (accelerating creep). They correspond to a decreasing, constant, and increasing strain rates, respectively [18]. A single equation (or model) cannot capture all the stages of the creep curve of a given material. To add more to its complexity, there are different creep curves for different temperatures and stresses, i.e., the creep strain is a function of time, temperature, and stress.

For our analysis, a modified time hardening (primary) creep model is chosen in ANSYS:

$$\varepsilon_{cr} = \frac{c_1 \sigma^{c_2} t^{c_3+1}}{c_3+1}, \qquad c_1 > 0, \tag{1}$$

where ε_{cr} is the equivalent creep strain, σ is the equivalent stress, t is time, and c_1, c_2, and c_3 are constants to be determined by curve fitting with experimental data. Using the experimental creep data for SA533B1 from Rempe et al. [9], the coefficients, as summarized

in Table 1, are generated for different temperatures. An example of the ANSYS creep model validation at temperature T = 1150 K with a stress of 26.5 MPa is given in Figure 5.

Table 1. Coefficients of the modified time hardening given in Eqn. 1 for different temperatures

Temperature [K]	900	1050	1150	1250	1373
c_1	1.461×10^{-31}	1.867×10^{-42}	7.801×10^{-28}	3.497×10^{-44}	5.383×10^{-47}
c_2	3.0881	4.8171	3.0886	5.5237	6.2092
c_3	-0.0560	0.1609	-0.0180	-0.1219	-0.0554

As a validation test, a uniaxial structural creep analysis was performed with a rectangular block (1 m × 0.2 m) at constant temperature T = 1150 K, clamped on one end, and applied stress of 26.5 MPa on the opposite end. The time-step (10 s), mesh edge size (0.04 m), and all other relevant input parameters discussed above are also used in the numerical validation. It is found that the standard norm of the difference between the numerical calculation and theory (Equation 1) is 0.4 % strain. Additional tests with uniform mesh edge sizes of 0.1 m and 0.02 m also yielded the same norms of about 0.4 % strain. On the other hand, the norm of the difference between the experiment and theory (Equation 1) is 3.6 % strain. However, neglecting in comparison by the data which is clearly in tertiary stage (the percent strain above 20 % in Figure 5), the norm of the difference between the experiment and theory is 2.3 %.

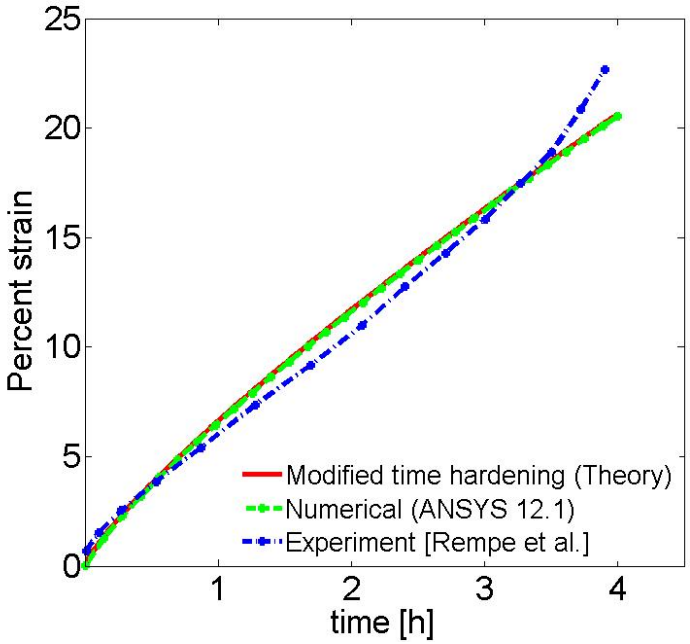

Figure 5. ANSYS creep model validation results for a rectangular block, set at constant temperature, clamped on one end, and an applied stress on the opposite end. The material is SA533B1 steel at T = 1150 K with a stress of 26.5 MPa. The experimental data is taken from Rempe et al. [9], and the ANSYS model is modified time hardening (primary creep) given in Eqn. 1.

In this study, we will not identify a yield or creep limit. This is motivated by the fact that creep is a thermally activated process and the material starts to creep even under moderate stresses lying below the yield limit [19]. In addition, the existence of a creep limit cannot be

verified experimentally at high temperatures since the main creep mechanism for metals and alloys is the diffusion of vacancies [20]. Therefore, we define a range of percent strain that can be considered as reliably predicted by the model. Beyond this range the results are only considered in a qualitative manner, meaning, that failure may happen in this stage but we cannot infer the time and deformations at which it happens. Specifically, we consider strains within 20 % as reliably predicted, which is partly based on the experimental creep data and the primary creep model that we use. The time necessary to reach 20 % strain defines the time frame when vessel integrity can be argued positively.

2. Results and discussion

A coupled thermo-mechanical creep analysis of the pressure vessel lower head or a part of it such as an IGT section can provide insights into modes of failure of the pressure vessel. In this section, we present results of two consecutive calculations and demonstrate that timing is a crucial parameter in defining dominant vessel failure modes in Nordic BWRs. We show that relative timing of global vessel failure, failure of the IGT nozzle welds, and clamping of the IGT in the IGT housing flow limiter define the dominant mode of vessel failure. First, a coupled thermo-mechanical creep analysis of a 2D axisymmetric model of the pressure vessel lower head is performed to determine the global vessel deformation, timing and mode of failure. Secondly, taking into account results from the first calculation, a coupled thermo-mechanical creep analysis is performed on a 3D IGT section to show that the IGT can fail before the global vessel wall failure takes place.

2.1 Global vessel deformation and failure

Figure 7 shows the von Mises creep strains and displacements of the vessel wall. Initially at time t = 0, the temperature of the vessel wall is set at 394 K and the melt pool depth that corresponds to the thermo-mechanical load is 1.9 m which is roughly 200 tons of debris. At time t = 3.06 h in Figure 7a, the maximum creep strain has reached 0.012 located in the vicinity of the top of the melt pool. The maximum displacement is 30 mm, but the displacement of the lower part of the vessel is almost uniform. High creep strains are localized in the region right below the pool top surface as can be seen in Figure 7b at time t = 3.33 h. The maximum creep strain has increased to 0.013 while the maximum displacement has increased to 36 mm. Further in time at t = 3.61 h, the 'localized creep' intensifies in the same location as shown in Figure 7c with a magnified view. This localized creep mode of failure is different from a 'ballooning' mode of failure observed in [8] for a shallower melt pool depth of 0.7 m.

Figure 9 shows the vertical displacement of the bottom center of the reactor. We divided the plot into two parts (i) solid line which represent reliably predicted results with less than 20 % strain, and (ii) dotted line which is beyond reliably predicted strain and can be considered only qualitatively. The vertical displacement follows a gradual growth to about 34 mm up to about 3.31 h in time. After about t = 3.31 h, the vertical displacement accelerates rapidly which also marks the increase of the maximum creep strain. As stated previously, we consider failure of the global vessel wall to happen when the maximum creep strain goes beyond 20 % but cannot infer exactly the time of failure and the corresponding deformations. However, once the maximum creep strain follows an accelerated increase, failure of the global vessel wall is considered imminent. Global vessel deformation and timing of the global vessel failure are the most important parameters for the next analysis of possible failure of an IGT before an occurrence of a global vessel failure.

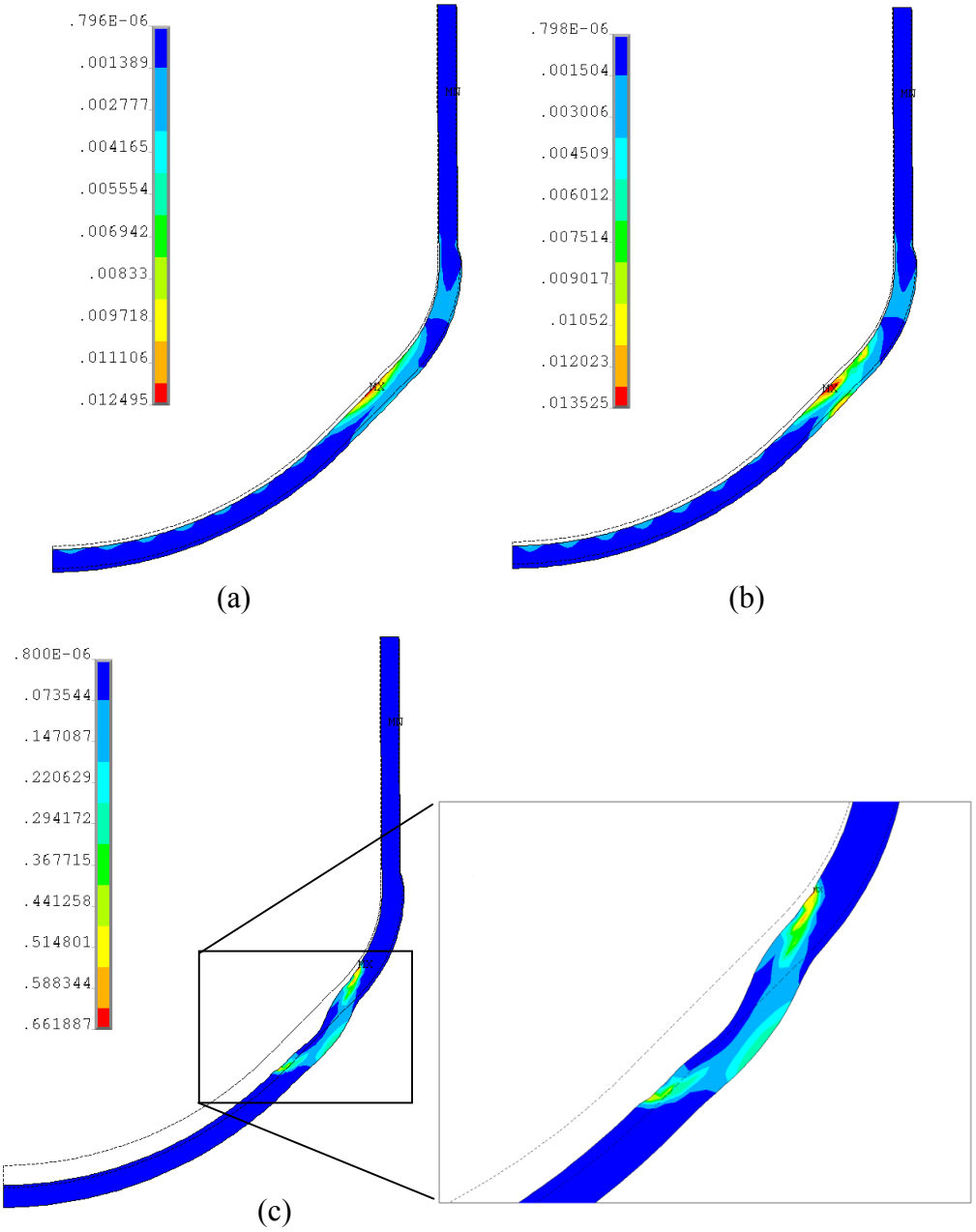

Figure 7. von Mises creep strains and displacements with melt pool depth H = 1.9 m at (a) 3.06 h, (b) 3.33 h, and (c) 3.61 h with a close-up of the localized creep region. The maximum displacements are (a) 30 mm, (b) 36 mm, and (c) 168 mm.

Elmir L
Delete

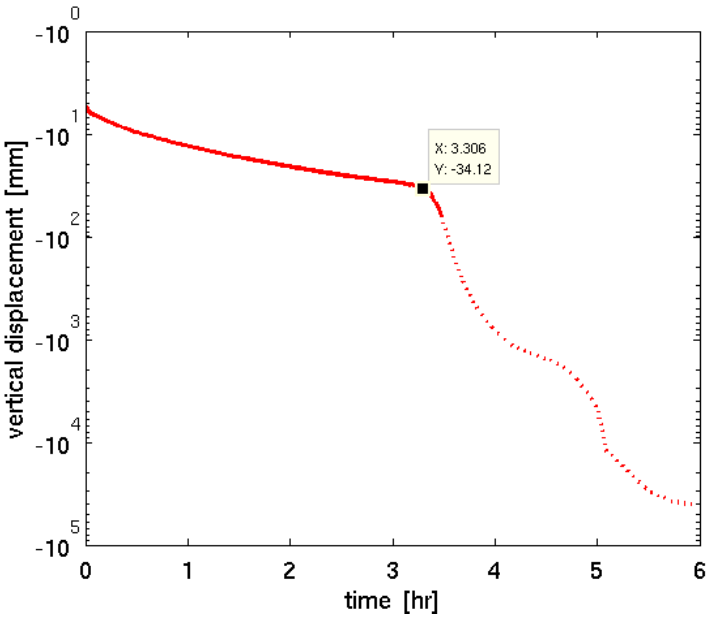

Figure 9. Vertical displacement of the bottom center of the lower plenum. The solid lines indicate reliable results that correspond to maximum creep strains within 20 %. The vertical displacement follows a rapid decrease after about 3.31 h (see marked data point).

Elmir L
Delete

2.2 Instrumentation guide tube failure

The global vessel wall deformation is taken into account in the local IGT section thermo-mechanical creep analysis as boundary conditions. Horizontal displacements of the right edge of the corresponding section from the 2D global vessel wall (see marked 'S' in Figure 1a) are imposed on the right surface of the 3D local IGT section (see Figure 3a). The constraint, $u_x = 0$ is imposed on the vertical symmetry axis (the left edge of the section from the 2D global vessel wall and on the 3D local IGT section). Vertical displacements of the left and right edges of the section from the 2D global vessel wall are almost identical up to 3.5 h (which is within the physical time of 3D local IGT analysis). Hence the left and right sides of the 3D local IGT section are both constrained with $u_y = 0$. The primary goal of the local IGT section thermo-mechanical creep analysis is to clarify if the IGT might fail before a global vessel wall failure takes place. The IGT is welded to the top of the IGT housing nozzle. When the nozzle is surrounded by high temperature corium debris, the nozzle welds can undergo creep and then melting. The time of IGT nozzle welds creep acceleration, $t = 1.25$ h, is determined from the slice-3D PECM calculation described previously, as well as the time of nozzle welds melting at $t = 2.64$ h (both plotted in Figure 8). A preliminary 3D unit volume PECM calculation has been performed for a rectangular 3D segment of the pool, containing one IGT in the center and surrounded by 4 CRGTs in the corners, to confirm the times of IGT nozzle welds creep acceleration and melting. The times of nozzle welds creep acceleration are consistent with a difference of about 100 s but the nozzle welds melting happens later, around $t = 3$ h in the 3D unit volume calculation. The 3D unit volume PECM simulation results also show that the temperature of the nozzle welds is much higher than the vessel wall temperature and indicate that the nozzle welds can fail before the vessel wall failure.

Elmir L
Delete
Elmir L
Delete

Now, our aim is to determine if clamping of the IGT occurs before the nozzle welds fail. The clamping possibility is attributed to thermal expansion of the vessel under the thermal load which can cause closure of a small gap between IGT and flow limiter in the IGT housing. If clamping does not happen before the nozzle welds fail, the IGT might get ejected from the housing. If this mode of vessel failure occurs earlier than the global vessel wall failure, e.g.,

ballooning type or localized creep [8], then melt can escape through the IGT housing reducing thermo-mechanical load on the vessel and thus hindering development of the global vessel failure.

In this study, we have considered only one melt pool depth at 1.9 m and one location of the IGT which is closest to the bottom center (see Figure 1 and Figure 3). Figure 11 shows the temperature profiles of the IGT section at different times with applied temperature at the top surface taken from the PECM calculations of local heat transfer in the segment of the pool containing one IGT and four CRGTs. In Figure 11a, the temperature profile at time t = 1.39 h is shown. The applied temperature at the top surface falls within 640 – 690 [K]. The temperature in the vicinity of the bottom area, where the flow limiter is located, is relatively uniform around 578 [K]. In Figure 11b the applied temperature at time t = 2.5 h has increased to within 800 – 885 [K] while the temperature in the vicinity of the flow limiter area has also increased to about 730 [K]. Volume expansion is observed at the top and bottom of the IGT section but in the scale that cannot be seen clearly in the scale of the figure. The applied normal displacement on the right curve-surface boundary is more visible in Figure 11b.

(a)

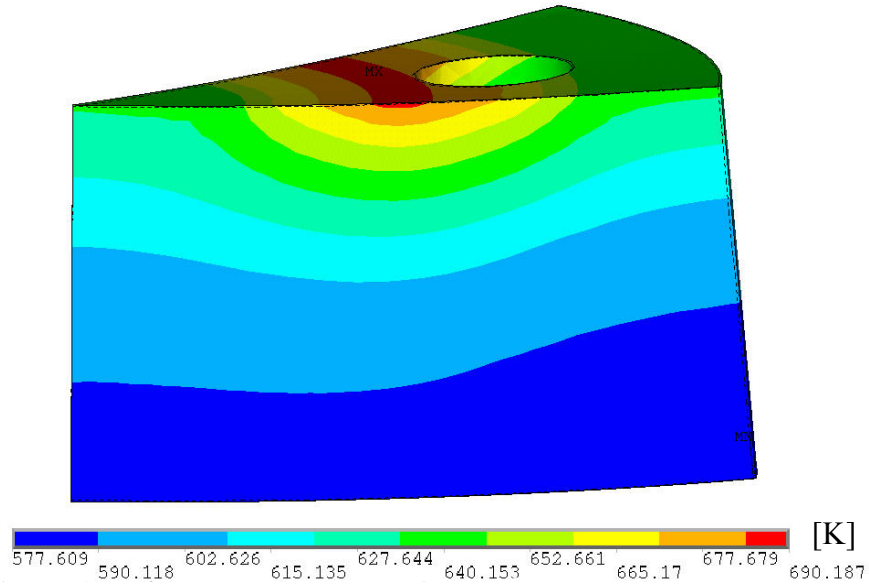

(b)

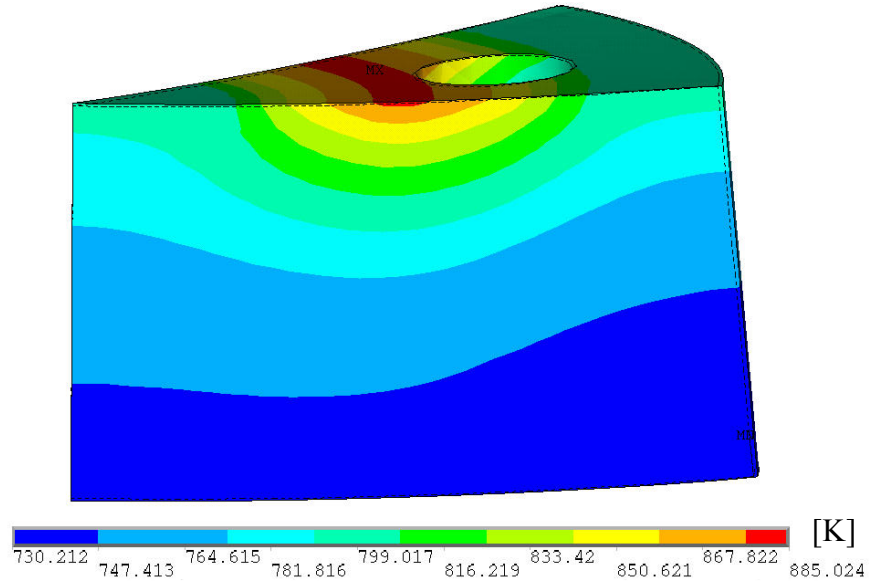

Figure 11. Temperature profiles at times t = 1.39 h and 2.5 h.

Figure 13a shows the displacement of the IGT housing points in a horizontal cross section of the flow limiter at times t = 1.39 h and 2.5 h. There are two attributing factors that can affect the displacement of the flow limiter area: (i) thermal expansion due to local thermal load, and (ii) applied displacement (normal to the right curved-surface boundary) as consideration of the global displacement of the vessel lower head. Figure 13a shows the trend in the displacement with respect to time as illustrated with the arrows. The direction of the applied displacement on the boundary is parallel to these arrows, which indicates that the global displacement of the lower head dominates over thermal expansion in the behavior of the flow limiter area.

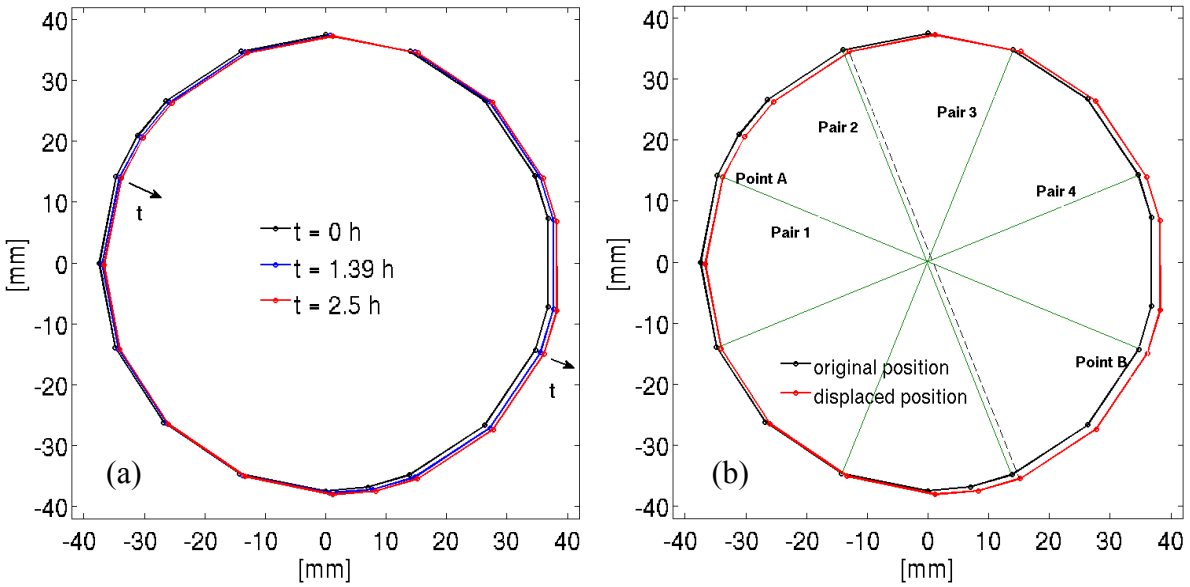

Figure 13. (a) Displacement of points along the flow limiter area at times t = 1.39 h and 2.5 h. (b) Clamping pairs in the flow limiter area. Each pair has two points from the flow limiter periphery, e.g., Pair 1 has points A and B. Four clamping pairs are considered and distances between points in each pair are measured with respect to time; see dashed line in the figure as an example showing the distance $D_2(t)$ between the points of Pair 2 at 2.5 h.

In Figure 13b a set of points in the flow limiter area are paired where the line connecting the points intersect the center of the ring initially, e.g., Pair 1 has points A and B. Four 'clamping pairs' are considered and distances between points in each pair are measured in time. The dashed line in the figure gives the distance $D_2(t)$ between the points of Pair 2 at 2.5 h. Then, in Figure 15, the change in distances $\Delta D_i(t) = D_i(t) - D_i(t_0)$ are plotted for each pair *i* and time t where $D_i(t_0)$ is the distance between the points in pair *i* at time t = 0. The maximum distance between the edge of the flow limiter and the IGT casing is given at 0.5 mm, which gives the 'clamping threshold' at -0.5 mm. More clearly, the separation distance between the points in any pair should shrink by at least 0.5 mm for the IGT casing to be clamped. Also that clamping should happen before the nozzle welds failure takes place, otherwise the IGT could get ejected from its housing first. Thus, clamping is defined as $\Delta D_i(t) \leq -0.5$ mm, for any pair *i* at any time $t > 0$ but before the nozzle welds fail.

In Figure 15, timing of the nozzle welds creep acceleration, and nozzle welds melting are plotted according to results of the slice-3D PECM calculation, while the previous calculation in Section 2.1 provided the timing of the global vessel wall creep acceleration. Analysis of results presented in Figure 15 suggest that at given melt pool depth of 1.9 m and a location of

the IGT close to the bottom center, the IGT is not clamped in its housing during the entire time until global vessel wall failure takes place. Other melt pool depths and/or other locations of the IGT might result otherwise, but are not covered here and will be the subject of further inquiry. Nevertheless, the results demonstrate that in the considered case of 1.9 m melt pool, the dominant vessel failure mode is IGT failure and it happens at least 1 h before the global vessel failure. It should be noted that the consequences of an IGT failure in the event of ex-vessel melt release and coolability is quite different from a global vessel wall failure in terms of size of the breach, amount of melt that can be released at once, and so on.

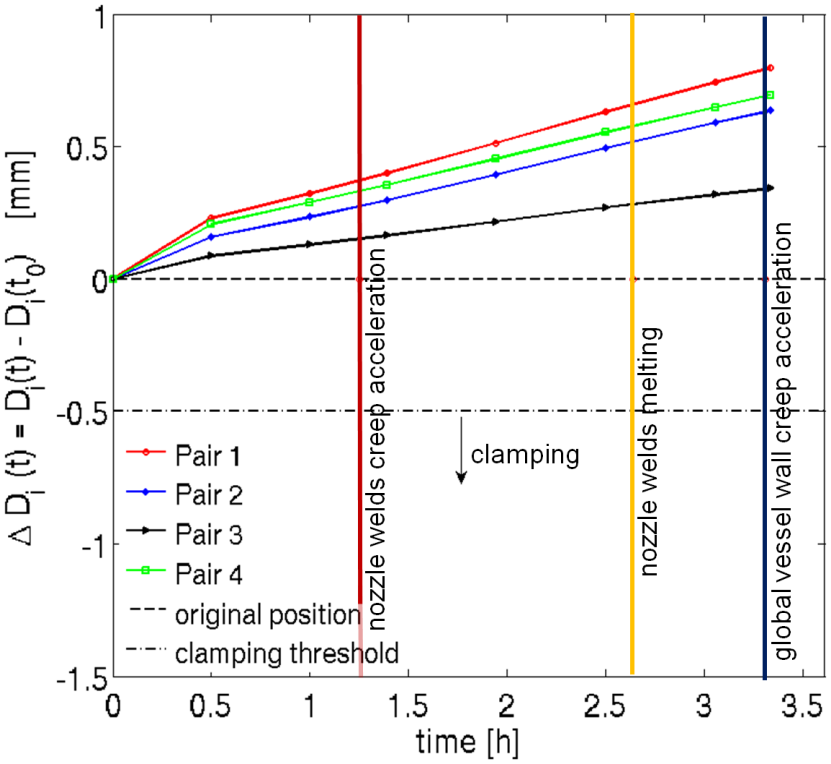

Figure 15. The change in distances $\Delta D_i(t) = D_i(t) - D_i(t_0)$ for each pair i and time t where $D_i(t_0)$ is the distance between the points in pair i at time t = 0. The clamping threshold is -0.5 mm which is equal to twice the distance between the flow limiter and the IGT casing given at 0.25 mm. The vertical lines correspond to the estimated time of nozzle welds creep acceleration, nozzle welds melting, and global vessel wall creep acceleration, that are seen, respectively from left to right. Clamping is defined as $\Delta D_i(t) \leq -0.5$, for any pair i at any time $t > 0$ but before the nozzle welds fail.

Elmir L
Delete

3. Conclusion

The present study addresses a hypothetical severe accident in a BWR with relocation of molten core materials to the lower head and subsequent debris bed melt pool formation. The melt pool formation in the lower head causes thermal and mechanical loads which can induce thermal creep failure of the reactor vessel wall and/or penetrations.

Two succeeding calculations were performed, a thermo-mechanical creep analysis for lover-head of the vessel wall and then for an IGT section. We have considered the maximum melt pool depth of 1.9 m and one location of the IGT that is closest to the center of the lower plenum. In the first calculation, we have found a localized creep mode of global vessel wall failure where creep strains are concentrated in the vicinity of the uppermost region of the melt

pool. Results of global vessel deformation and timing of failure from this calculation as well as local transient thermal load from PECM calculations are then used for the next analysis of the IGT section. We have found that the IGT casing is not clamped in the flow-limiter gap the entire time. Since the IGT nozzle welds fail at least 1 h before the global vessel wall does, the IGT failure is considered as the dominant vessel failure mode. We should also mention that preliminary calculations with smaller depth pools indicate that an opposite behavior can be also observed. Namely a contraction of the flow limiter gap might lead to clamping of the IGT in its housing. In future work, we plan to consider different melt pool depths and other locations of the IGT to determine the dependency of IGT failure on these parameters.

The methodology that is used here can also be implemented to analyze possible modes of structural failure of other parts of the BWR lower plenum such as the CRGTs, nozzle pumps, and drain tubes. An important future step for further improvement in the current methodology is full 3D modeling of global deformation of the vessel taking into account penetrations.

4. Acknowledgements

The work is supported by the Swedish Nuclear Radiation Protection Authority (SSM), Swedish Power Companies, European Commission (SARNET-2), Nordic Nuclear Safety Program (NKS), and Swiss Federal Nuclear Safety Inspectorate (ENSI) under the APRI-MSWI program at the Royal Institute of Technology (KTH), Stockholm, Sweden.

5. References

[1] P. Kudinov, A. Karbojian, W. Ma, and T.-N. Dinh "The DEFOR-S Experimental Study of Debris Formation with Corium Simulant Materials", *Nuclear Technology*, Vol. 170, No. 1, 2010, pp. 219-230.

[2] P. Kudinov, A. Karbojian, and C.-T. Tran, "Experimental Investigation of Melt Debris Agglomeration with High Melting Temperature Simulant Materials," Proceedings of ISAMM-2009, Böttstein, Switzerland, 2009 October 26 - 28.

[3] P. Kudinov and M. Davydov, "Approach to Prediction of Melt Debris Agglomeration Modes in a LWR Severe Accident," Proceedings of ISAMM-2009, Böttstein, Switzerland, 2009 October 26 - 28.

[4] S. Yakush, P. Kudinov, and T.-N. Dinh, "Multiscale Simulations of Self-organization Phenomena in the Formation and Coolability of Corium Debris Bed," Proceedings The 13th International Topical Meeting on Nuclear Reactor Thermal Hydraulics (NURETH-13), Kanazawa City, Ishikawa Prefecture, Japan, Paper N13P1143, 2009 September 27-October 2.

[5] S. Yakush and P. Kudinov, "Simulation of Ex-Vessel Debris Bed Formation and Coolability in a LWR Severe Accident," Proceedings of ISAMM-2009, Böttstein, Switzerland, 2009 October 26 - 28.

[6] D. Magallon, K.H. Bang, S. Basu, G. Berthoud, M. Bürger, M.L. Corradini, H. Jacobs, O. Melikhov, K. Moriyama, M. Naitoh, J.H. Song, N. Suh, and T.G. Theofanous, "FCI phenomena uncertainties impacting predictability of dynamic loading of reactor structures (SERENA programme)," Proceedings Workshop on Evaluation of Uncertainties in Relation to Severe Accidents and Level 2 Probabilistic Safety Analysis, Hotel Aquabella, Aix-en-Provence, France, 2005 November 7–9.

[7] H.-G. Willschuetz, E. Altstadt, B. R. Sehgal, and F.-P. Weiss, "Recursively coupled thermal and mechanical FEM-analysis of lower plenum creep failure experiments", *Annals of Nuclear Energy*, Vol. 33, 2006, pp. 126-148.

[8] W. Villanueva, C.-T. Tran, and P. Kudinov, "Coupled thermo-mechanical creep analysis for boiling water reactor lower head", Proceedings of the 8th International Topical Meeting on Nuclear Thermal Hydraulics, Operation and Safety (NUTHOS-8), Shanghai, China, Paper N8P0248, 2010 October 10-14.

[9] J. L. Rempe, S. A. Chavez, G. L. Thinnes, C. M. Allison, G. E. Korth, R. J. Witt, J. J. Sienicki, S. K. Wang, L. A. Stickler, C. H. Heath, and S. D. Snow, *Light Water Reactor Lower Head Failure*, Report NUREG/CR-5642, Idaho Falls, 1993.

[10] K. Ikonen, "Mechanical analysis of Olkiluoto RPV bottom in core melting accident", VTT Research Report, PRO1/7017/04, 2004.

[11] C.-T. Tran, T.-N. Dinh, "The effective convectivity model for simulation of melt pool heat transfer in a light water reactor pressure vessel lower head. Part I: Physical processes, modeling and model implementation", *Progress in Nuclear Energy*, Vol. 51, 2009, pp. 849-859.

[12] http://www.fluent.com/, 2011 March.

[13] http://ansys.com/, 2011 March.

[14] ANSYS 13, *User's Manual*, ANSYS®, Inc., 2010.

[15] V. A. Bui and T.-N. Dinh, "Modeling of heat transfer in heated-generating liquid pools by an effective diffusivity-convectivity approach", Proceedings of 2nd European Thermal-Sciences Conference, Rome, Italy, 1996, pp. 1365-1372.

[16] U. Steinberner and H. H. Reineke, "Turbulent buoyancy convection heat transfer with internal heat sources", Proceedings of the 6th International Heat Transfer Conference, Toronto, Canada, 1978, pp. 305-310.

[17] C.-T. Tran and T.-N. Dinh, "The effective convectivity model for simulation of melt pool heat transfer in a light water reactor lower head. Part II: Model assessment and application", *Progress in Nuclear Energy*, Vol. 51, 2009, pp. 860-871.

[18] E. Andrade, "The viscous flow in metals and allied phenomena", *Proc. R. Soc. London A*, Vol. 84, 1910, pp. 1-12.

[19] K. Naumenko and H. Altenbach, *Modeling of Creep for Structural Analysis*, Springer-Verlag, Berlin, Germany, 2007.

[20] H. J. Frost and M. F. Ashby, *Deformation-Mechanism Maps: The Plasticity and Creep of Metals and Ceramics*, Pergamon, Oxford, UK, 1982. http://engineering.dartmouth.edu/defmech.